We are IntechOpen, the world's leading publisher of Open Access books Built by scientists, for scientists

6,900
Open access books available

186,000
International authors and editors

200M
Downloads

Our authors are among the

154
Countries delivered to

TOP 1%
most cited scientists

12.2%
Contributors from top 500 universities

WEB OF SCIENCE™

Selection of our books indexed in the Book Citation Index
in Web of Science™ Core Collection (BKCI)

Interested in publishing with us?
Contact book.department@intechopen.com

Numbers displayed above are based on latest data collected.
For more information visit www.intechopen.com

Robust Interferometric Phase Estimation in InSAR via Joint Subspace Projection

Hai Li and Renbiao Wu
Tianjin Key Lab for Advanced Signal Processing,
Civil Aviation University of China, Tianjin,
P.R. China

1. Introduction

Synthetic aperture radar interferometry (InSAR) is an important remote sensing technique to retrieve the terrain digital elevation model (DEM)[1][2]. Image coregistration, InSAR interferometric phase estimation (or noise filtering) and interferometric phase unwrapping[3][4][5][6] are three key processing procedures of InSAR. It is well known that the performance of interferometric phase estimation suffers seriously from poor image coregistration.

Image coregistration is an important preprocessing operation that aligns the pixels of one image to the corresponding pixels of another image. A review of recent as well as classic image registration methods can be found in Ref.[7]. Mutual information used for the registration of remote sensing imagery are presented in the literature[8]. In literature[9], the feature-based registration methods are presented. A new direct Fourier-transform-based algorithm for subpixel registration is proposed in Ref.[10]. In Ref.[11], a geometrical approach for image registration of SAR images is proposed, and the algorithm has been tested on several real data. A image registration method based on isolated point scatterers is proposed in Ref.[12].

Almost all the conventional InSAR interferometric phase estimation methods are based on interferogram filtering[13][14][15][16][17][18], such as pivoting mean filtering[13], pivoting median filtering[14], adaptive phase noise filtering[15], and adaptive contoured window filtering[18]. However, when the quality of an interferogram is very poor due to a large coregistration error, it is very difficult for these methods to retrieve the true terrain interferometric phases. In fact, the interferometric phases are random in nature with their variances being inversely proportional to the correlation coefficients between the corresponding pixel pairs of the two coregistered SAR images[2]. Therefore, the terrain interferometric phases should be estimated statistically.

In this chapter, the interferometric phase estimation method based on subspace projection and its modified version were proposed. Theoretical analysis and computer simulation results show that the methods can provide accurate estimation of the terrain interferometric phase (interferogram) even if the coregistration error reaches one pixel. The remainder of this chapter is organized as follows. Section 2 presents the signal model of a single pixel pair

and the problem formulation. In Section 3, we discuss the interferometric phase estimation method based on subspace projection. In Section 4, the modified interferometric phase estimation method via subspace projection is presented in details. Finally, numerical and experemental results are presented in Section 5. Section 6 concludes the whole chapter.

2. Data model and problem formulation

Assuming that the SAR images are accurately coregistered and the interferometric phases are flattened with a zero-height reference plane surface. The complex data vector, denoted as $\mathbf{s}(i)$, of a pixel pair i (corresponding to the same ground area) of the coregistered SAR images can be formulated as follows[19],

$$\mathbf{s}(i) = [s_1(i), s_2(i)]^{\mathrm{T}} = \mathbf{a}(\varphi_i) \odot [x_1(i), x_2(i)]^{\mathrm{T}} + \mathbf{n}(i) = \mathbf{a}(\varphi_i) \odot \mathbf{x}(i) + \mathbf{n}(i) \tag{1}$$

where $\mathbf{a}(\varphi_i) = [1, e^{j\varphi_i}]^T$ is the spatial steering vector (i.e., the array steering vector) of the pixel i, superscript T denotes the vector transpose operation, φ_i is the terrain interferometric phase to be estimated, $\odot$ denotes the Hadamard product, $\mathbf{x}(i)$ is the complex magnitude vector (i.e., complex reflectivity vector of scene received by the satellites) of the pixel i, and $\mathbf{n}(i)$ is the additive noise term. The complex data vector $\mathbf{s}(i)$ can be modeled as a joint complex circular Gaussian random vector with zero-mean and the corresponding covariance matrix $\mathbf{C}_s(i)$ is given by

$$\begin{aligned}
\mathbf{C_s}(i) &= E\{\mathbf{s}(i)\mathbf{s}^H(i)\} \\
&= \mathbf{a}(\varphi_i)\mathbf{a}^H(\varphi_i) \odot E\{\mathbf{x}(i)\mathbf{x}^H(i)\} + \sigma_n^2 \mathbf{I} \\
&= \sigma_s^2(i)\mathbf{a}(\varphi_i)\mathbf{a}^H(\varphi_i) \odot \mathbf{R}_s(i) + \sigma_n^2 \mathbf{I}
\end{aligned} \tag{2}$$

$$\mathbf{R}_s(i) = \begin{bmatrix} r_{11}(i), & r_{12}(i) \\ r_{21}(i), & r_{22}(i) \end{bmatrix} \tag{3}$$

where $\mathbf{R_s}(i)$ is called the correlation coefficient matrix, $\mathbf{I}$ is a 2×2 identity matrix, $r_{mn}(i)$ ($0 \le r_{mn}(i) \le 1$, $n = 1,2$, and $m = 1,2$) are the correlation coefficients between the satellites m and n, $E\{\}$ denotes the statistical expectation, superscript H denotes vector conjugate-transpose, $\sigma_s^2(i)$ is the echo power of the pixel i and σ_n^2 is the noise power. In order to simplify the mathematical expressions, the denotation i (denoting the pixel) in the right side of the following expressions is omitted. In practice, the statistical covariance matrix of (2) can be adaptively estimated using the sample covariance matrix.

If the SAR images are accurately coregistered and the cross-correlation coefficients (i.e., the nondiagonal elements) of $\mathbf{R}_s(i)$ are large enough, the number of the principal eigenvalues of the covariance matrix $\mathbf{C}_s(i)$ is one; i.e., the dimensions of the signal subspace and the noise subspace are both one (in the absence of the layover). In this case, the eigen-decomposition of the covariance matrix $\mathbf{C}_s(i)$ is as follows:

$$\mathbf{C_s}(i) = (\lambda_{rs} + \sigma_n^2)(\mathbf{a}(\varphi_i) \odot \boldsymbol{\beta}_{rs})(\mathbf{a}(\varphi_i) \odot \boldsymbol{\beta}_{rs})^H + \sigma_n^2 \boldsymbol{\beta}_n \boldsymbol{\beta}_n^{\ H} \tag{4}$$

where λ_{rs} and β_{rs} are the principal eigenvalue and the corresponding eigenvector (i.e., the signal eigenvector) of $\mathbf{R}_s(i)$, respectively, and β_n is the noise eigenvector corresponding to the insignificant eigenvalue of $\mathbf{C}_s(i)$. From (4) we can note that $(\mathbf{a}(\varphi_i) \odot \beta_{rs})$ is in the signal subspace, β_n is in the noise subspace, and $(\mathbf{a}(\varphi_i) \odot \beta_{rs})$ are orthogonal to β_n, which is used to estimate the interferometric phase φ_i.

The definition of cost function is,

$$J_1 = (\mathbf{a}(\varphi_i) \odot \beta_{rs})^H \beta_n \beta_n^H (\mathbf{a}(\varphi_i) \odot \beta_{rs}) \qquad (5)$$

The minimization of J_1 can provide the optimum estimate of the interferometric phase φ_i.

The eigenvalues of $C_s(i)$ result in a low dispersion due to the increase of the coregistration error. Actually, it is induced by the increase of noise eigenvalue, i.e., the signal component spreads into the noise space. Moreover, the 2-dimensional space will be fully occupied by signal component with a worse coregistration error of one pixel. At this instant, the noise eigenvalue is almost equal to the bigger one. The noise subspace dimension becomes zero. The degree of the signal component spreading to the noise subspace is smaller, the estimation of the InSAR interferometric phase is better(the subspace projection technique is used to estimate the InSAR interferometric phase). On the contrary, the degree of the signal component spreading to the noise subspace is larger, the estimation of the InSAR interferometric phase is worse. The conclusions obtained from the preceding analysis are briefly summarized as follows: the degree of the signal component spreading to the noise subspace becomes larger and larger as the coregistration error increases when the example of formula (1) is used to build the data vector. In other words, the degree of dispersion is heavily impacted by the coregistration error. The simulation result shown in Fig.1 demonstrates the above conclusions.
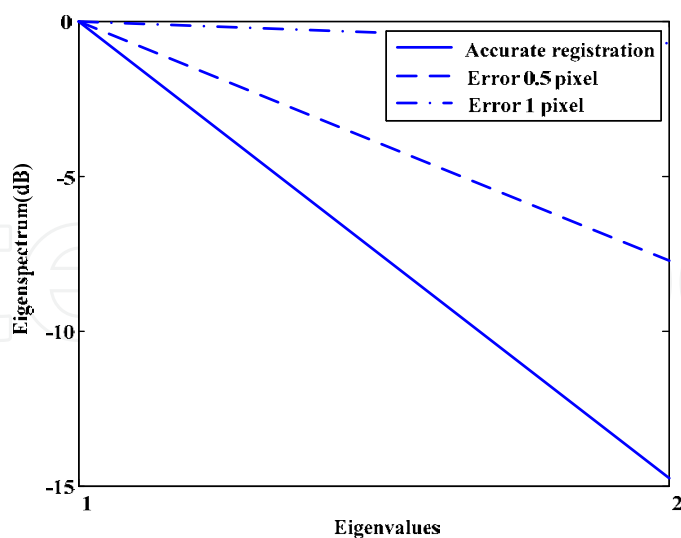

Fig. 1. Eigenspectra of the covariance matrix for accurate coregistration, coregistration errors of 0.5 and 1 pixels, respectively.

The cost function given by (5) can be used to estimate the InSAR interferometric phase when the SAR images are accurately coregistered. However, in the presence of coregistration

error, the cross-correlation coefficients are smaller than 1 and the noise eigenvalue becomes large. In the completely misregistered case, the rank of $\mathbf{R_s}(i)$ becomes 2, which means that the noise subspace vanishes in the eigenspace of $\mathbf{C}_s(i)$. So the cost function given by (5) can not be used to estimate the InSAR interferometric phase in the presence of coregistration error.

3. Interferometric phase estimation via subspace projection

Considering the difficulties in accurate coregistration, we use not only the corresponding pixel pair i of the coarsely coregistered SAR image pair (as given in (1)) but also the neighboring pixel pairs centered on the pixel pair i to jointly construct the data vector. An example of the construction method for the data vector is shown in Fig.2, where a circle represents a SAR image pixel and i denotes the centric pixel pair (i.e., the desired pixel pair whose interferometric phase is to be estimated). We call this extended data vector $\mathbf{si}(i)$ the joint data vector. The number of the neighboring pixel pairs to construct the joint data vector is 8 as shown in Fig.2.
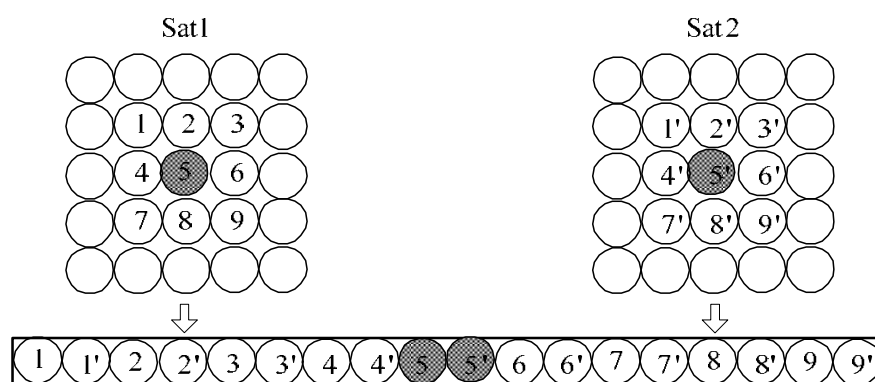

Fig.2. A construction method for the joint data vector.

The joint data vector $\mathbf{si}(i)$ as shown in Fig.2 can be written as:

$$\mathbf{si}(i) = [\mathbf{s}(i-4)^T, \mathbf{s}(i-3)^T, \cdots, \mathbf{s}(i)^T, \cdots, \mathbf{s}(i+4)^T]^T \tag{6}$$

The corresponding joint covariance matrix is given by

$$\begin{aligned}\mathbf{C_{si}}(i) &= E\{\mathbf{si}(i)\mathbf{si}^H(i)\} \\ &= \boldsymbol{\alpha}(\varphi_{i-4}, \varphi_{i-3}, \cdots, \varphi_{i+4})\boldsymbol{\alpha}^H(\varphi_{i-4}, \varphi_{i-3}, \cdots, \varphi_{i+4}) \odot \mathbf{R_{si}}(i) + \sigma_n^2\mathbf{I}\end{aligned} \tag{7}$$

where $\boldsymbol{\alpha}(\varphi_{i-4}, \varphi_{i-3}, \cdots, \varphi_{i+4}) = [\mathbf{a}^T(\varphi_{i-4}), \mathbf{a}^T(\varphi_{i-3}), \cdots, \mathbf{a}^T(\varphi_{i+4})]^T$ and $\mathbf{R_{si}}(i)$ are referred to as the joint steering vector and the joint correlation function matrix of the pixel pair i, respectively. In fact, most of the nature terrain can be approximated by a local plane. After we estimate the local slopes and correct the neighboring pixels, we can assume that the neighboring pixels have the almost identical terrain height[20]. That is, the spatial steering vectors of the pixel pairs in $\mathbf{si}(i)$ are assumed to be identical, i.e., $\mathbf{a}(\varphi_{i-4}) = \mathbf{a}(\varphi_{i-3}) = \cdots = \mathbf{a}(\varphi_{i+4}) = [1, e^{j\varphi_i}]^T$ and $\boldsymbol{\alpha}(\varphi_{i-4}, \varphi_{i-3}, \cdots, \varphi_{i+4}) = [\mathbf{a}^T(\varphi_i), \mathbf{a}^T(\varphi_i), \cdots, \mathbf{a}^T(\varphi_i)]^T = [1, e^{j\varphi_i} \cdots, 1, e^{j\varphi_i}]^T$. The simplified joint

steering vector of the pixel i is denoted by $\mathbf{ai}(\varphi_i) = [\mathbf{a}^T(\varphi_i), \mathbf{a}^T(\varphi_i), \cdots, \mathbf{a}^T(\varphi_i)]^T$ (18×1). Substituting $\mathbf{ai}(\varphi_i)$ for $\boldsymbol{\alpha}(\varphi_{i-4}, \varphi_{i-3}, \cdots, \varphi_{i+4})$ in (7), we have,

$$
\begin{aligned}
\mathbf{C_{si}}(i) &= \mathbf{ai}(\varphi_i)\mathbf{ai}^H(\varphi_i) \odot \mathbf{R_{si}}(i) + \sigma_n^2 \mathbf{I} \\
&\underline{\underline{EVD}} \sum_{k=1}^{K} \lambda_{csi}^{(k)} \boldsymbol{\beta}_{csi}^{(k)} \boldsymbol{\beta}_{csi}^{(k)H} + \sum_{l=1}^{18-K} \sigma_n^2 \boldsymbol{\beta}_{nsi}^{(l)} \boldsymbol{\beta}_{nsi}^{(l)H} \\
&= \sum_{k=1}^{K} (\lambda_{rsi}^{(k)} + \sigma_n^2)(\mathbf{ai}(\varphi_i) \odot \boldsymbol{\beta}_{rsi}^{(k)})(\mathbf{ai}(\varphi_i) \odot \boldsymbol{\beta}_{rsi}^{(k)})^H + \sum_{l=1}^{18-K} \sigma_n^2 \boldsymbol{\beta}_{nsi}^{(l)} \boldsymbol{\beta}_{nsi}^{(l)H}
\end{aligned}
\tag{8}
$$

where K is the number of the principal eigenvalues of $\mathbf{C_{si}}(i)$, $\boldsymbol{\beta}_{csi}^{(k)}$ ($k = 1,2,\cdots,K$) are the eigenvectors corresponding to the principal eigenvalues $\lambda_{csi}^{(k)}$ of $\mathbf{C_{si}}(i)$, $\boldsymbol{\beta}_{rsi}^{(k)}$ ($k = 1,2,\cdots,K$) are the eigenvectors corresponding to the principal eigenvalues $\lambda_{rsi}^{(k)}$ of $\mathbf{R_{si}}(i)$. σ_n^2 and $\boldsymbol{\beta}_{nsi}^{(l)}$ ($l = 1,2,\cdots,18-K$) are the noise eigenvalue and the corresponding eigenvectors of $\mathbf{C_{si}}(i)$, respectively. From (8) we can note that $\mathbf{ai}(\varphi_i) \odot \boldsymbol{\beta}_{rsi}^{(k)}$ ($k = 1,2,\cdots,K$) are in the signal subspace of $\mathbf{C_{si}}(i)$, $\boldsymbol{\beta}_{nsi}^{(l)}$ ($l = 1,2,\cdots,18-K$) are in the noise subspace of $\mathbf{C_{si}}(i)$, and $\mathbf{ai}(\varphi_i) \odot \boldsymbol{\beta}_{rsi}^{(k)}$ are orthogonal to $\boldsymbol{\beta}_{nsi}^{(l)}$.

If the SAR images are accurately coregistered, the structure form of the joint correlation function matrix $\mathbf{R_{si}}(i)$ are given by

$$
\mathbf{R_{si}}(i) = \begin{bmatrix}
\sigma_s^2(i-4)\mathbf{R_s}(i-4) & 0 & \cdots & 0 \\
0 & \sigma_s^2(i-3)\mathbf{R_s}(i-3) & & \\
\vdots & & \ddots & \\
0 & & & \sigma_s^2(i+4)\mathbf{R_s}(i+4)
\end{bmatrix}
\tag{9}
$$

where $\mathbf{R_s}(m)$ and $\sigma_s^2(m)$ ($m = i-4, i-3, \cdots, i+4$) in the diagonal of the $\mathbf{R_{si}}(i)$ are the coherence coefficient matrix (given by (3)) and the echo power of the pixel pair m, respectively. We can notice from (9) that when the SAR images are accurately coregistered, only the elements in $\mathbf{R_s}(m)$ are nonzero, while all the other elements of $\mathbf{R_{si}}(i)$ (or $\mathbf{C_{si}}(i)$) are zero (assuming the complex reflectivity is independent from pixel to pixel and neglecting the noise). In other words, $\mathbf{R_{si}}(i)$ is a block diagonal matrix. However, if the SAR images are not accurately coregistered, the nonzero elements in the submatrices $\mathbf{R_s}(m)$ are diffused to other non-diagonal element positions of $\mathbf{R_{si}}(i)$, as shown in Fig.3(b) and Fig.3(c). The dimensions of the joint correlation function matrix $\mathbf{R_{si}}(i)$ are 18×18. Fig.3(a) is the structure of $\mathbf{R_{si}}(i)$ for accuracy coregistration; Fig.3(b) is the structure of $\mathbf{R_{si}}(i)$ for the coregistration error of 0.5 pixel; Fig.3(c) is the structure of $\mathbf{R_{si}}(i)$ for the coregistration error of 1 pixel. From Fig.3 we can see that when the SAR images are not accurately coregistered, the same imaged ground area can be coregistered to different pixel positions; thus its correlation information appears in other non-diagonal element position of $\mathbf{R_{si}}(i)$. The gray level denotes the magnitude of each element with the white strongest and black zero.

(a)   (b)   (c)
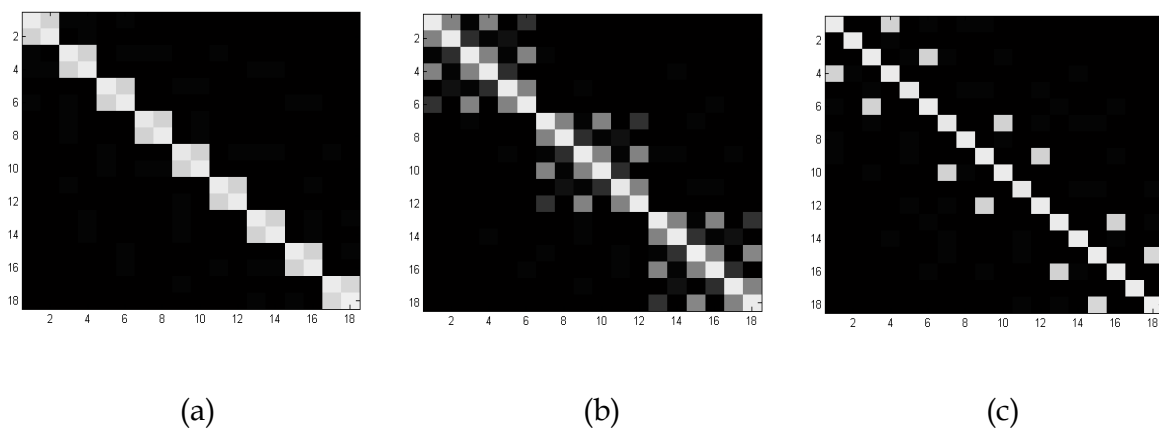
Fig. 3. Structures of joint correlation function matrix for different coregistration errors: (a) accurate coregistration; (b) coregistration error of 0.5 pixels; (c) coregistration error of 1 pixel.

Comparing Fig.3 with (4), the conventional estimation approaches based on the single pixel pair will be not feasible if the coregistration error is very large, for example, larger than 0.5 pixel, while our approach can still achieve the optimum estimation due to the use of multiple neighboring pixel pairs.

From the literature[21], we can know that: for the accurate coregistration, the dimensions of the signal subspace and the noise subspace of the joint covariance matrix $\mathbf{C_{si}}(i)$ (18×18) are both 9. For the coregistration error of 1 pixel, the dimensions of the signal subspace and the noise subspace of the joint covariance matrix $\mathbf{C_{si}}(i)$ are changed to 12 and 6, respectively. The method can also provide accurate estimation of the terrain interferometric phase even if the coregistration error reaches one pixel only by changing the dimension of the noise subspace from 9 to 6.

As mentioned above, the signal subspace $\mathbf{ai}(\varphi_i) \odot \boldsymbol{\beta}_{rsi}^{(k)}$ ($k = 1, 2, \cdots, K$) is orthogonal to the noise subspace $\mathbf{N_c} = span\{\boldsymbol{\beta}_{nsi}^{(1)}, \boldsymbol{\beta}_{nsi}^{(2)}, \cdots \boldsymbol{\beta}_{nsi}^{(M-K)}\}$, which is used to estimate the interferometric phase φ_i.

The definition of cost function is,

$$J_2 = \sum_{k=1}^{K} \sum_{l=1}^{M-K} (\mathbf{ai}(\varphi_i) \odot \boldsymbol{\beta}_{rsi}^{(k)})^H \boldsymbol{\beta}_{nsi}^{(l)} \boldsymbol{\beta}_{nsi}^{(l)H} (\mathbf{ai}(\varphi_i) \odot \boldsymbol{\beta}_{rsi}^{(k)}) \tag{10}$$

The minimization of J_2 can provide the optimum estimate of the interferometric phase φ_i.

Fig.s 4 shows the simulation results for various coregistration errors by the subspace projection method. Comparing these figures, we can observe that the large coregistration error has almost no effect on the interferograms obtained by the proposed method. We can see that the subspace projection method in this chapter is robust to large coregistration errors (up to one pixel).
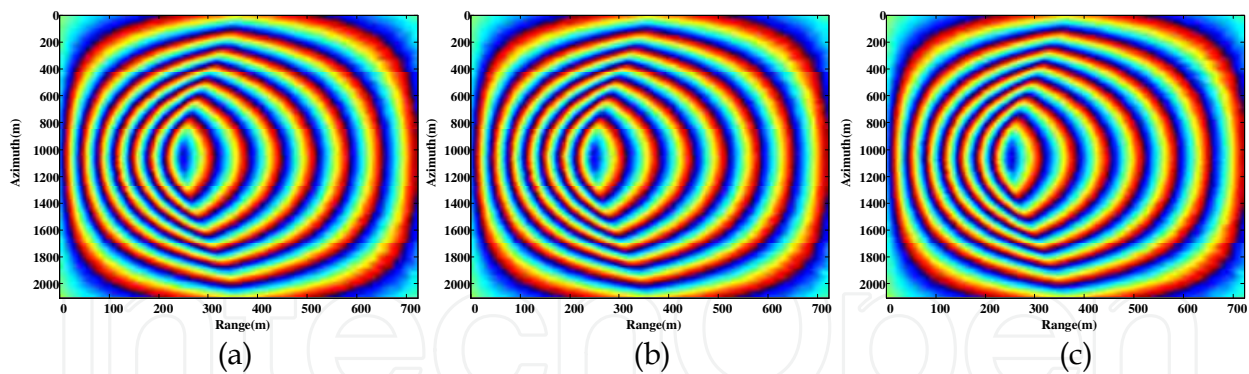
(a)   (b)   (c)

Fig. 4. The interferograms obtained by the subspace projection method for the accurate coregistration (a), the coregistration error of 0.5 pixels (b) and the coregistration error of one pixel (c).

4. Modified interferometric phase estimation via subspace projection

The joint subspace projection method mentioned above employs the projection of the joint signal subspace onto the corresponding joint noise subspace which is obtained from the eigendecomposition of the joint covariance matrix to estimate the terrain interferometric phase, and takes advantage of the coherence information of the neighboring pixel pairs to auto-coregister the SAR images, where the phase noise is reduced simultaneously. However, the noise subspace dimension of the covariance matrix changes with the coregistration error. For accurate estimating the InSAR interferometric phase, the noise subspace dimension of the covariance matrix must be known, and the performance of the method (i.e. subspace projection method) degrades when the noise subspace dimension is not estimated correctly. In this chapter, an modified joint subspace projection method for InSAR interferometric phase estimation is proposed. In this method, the benefit from the new formulation of joint data vector is that the noise subspace dimension of the covariance matrix is not affected by the coregistration error (i.e., the noise subspace dimension of the corresponding covariance matrix with the coregistration error μ ($0 < \mu \leq 1$) pixel is the same as that of the covariance matrix with accurate coregistration). So the method does not need to calculate the noise subspace dimension before estimating the InSAR interferometric phase.

4.1 Data modeling of the modified method

For avoiding the trouble of calculating the noise subspace dimension before estimating the InSAR interferometric phase, the new formulation of joint data vector is used in the proposed method. An example to construct the new joint data vector $\mathbf{si}(i)$ is shown in Fig.5.

The joint data vector $\mathbf{si}(i)$ shown in Fig.5 can be written as

$$\mathbf{si}(i) = [s_1(i-1), s_2(i-6), s_2(i-5), s_2(i-2), s_2(i-1), s_1(i), s_2(i-4), s_2(i-3), s_2(i), s_2(i+1),$$
$$s_1(i+3), s_2(i+2), s_2(i+3), s_2(i+6), s_2(i+7), s_1(i+4), s_2(i+4), s_2(i+5), s_2(i+8), s_2(i+9)]^T \quad (11)$$

The corresponding covariance matrix $\mathbf{C_{si}}(i)$ is given by

$$\begin{aligned}\mathbf{C_{si}}(i) &= E\{\mathbf{si}(i)\mathbf{si}^H(i)\} \\ &= \mathbf{ai}(\varphi_i)\mathbf{ai}^H(\varphi_i) \odot \mathbf{R_{si}}(i) + \sigma_n^2 \mathbf{I}\end{aligned}$$

$$(12)$$

where

$$\mathbf{ai}(\varphi_i) = \left[1, e^{j\varphi_i}, e^{j\varphi_i}, e^{j\varphi_i}, e^{j\varphi_i}, 1, e^{j\varphi_i}, e^{j\varphi_i}, e^{j\varphi_i}, e^{j\varphi_i}, 1, e^{j\varphi_i}, e^{j\varphi_i}, e^{j\varphi_i}, e^{j\varphi_i}, 1, e^{j\varphi_i}, e^{j\varphi_i}, e^{j\varphi_i}, e^{j\varphi_i}\right]^T$$ and

$\mathbf{R_{si}}(i)$ are referred to as the joint generalized steering vector and the joint correlation function matrix of the pixel pair *i*, respectively. The deduction of equation (12) is presented in appendix A.
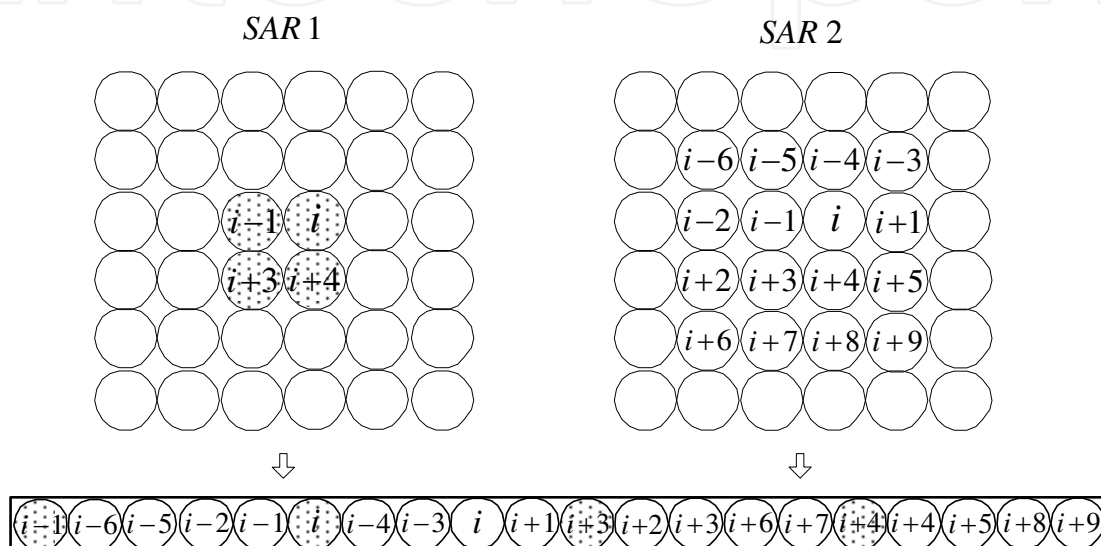

Fig. 5. Formulation of the joint data vector.

In the following the noise subspace dimension of the joint covariance matrix $\mathbf{C_{si}}(i)$ for different coregistration errors are discussed.

a. Accurate coregistration.

For the accurate coregistration, the joint data vector, $\mathbf{si}(i)$, that is shown in Fig.6, where circles represent SAR image pixels pair whose interferometric phase has to be estimated.

We can rearrange the elements (pixels) of $\mathbf{si}(i)$ to obtain $\mathbf{si}'(i)$ as shown in Fig.6, which does not change the eigenvalues of the corresponding covariance matrix[21]. The joint data vector $\mathbf{si}'(i)$, shown in Fig.6, can be written as

$$\begin{aligned}\mathbf{si}'(i) = [&s_1(i-1), s_2(i-1), s_1(i), s_2(i), s_1(i+3), s_2(i+3), s_1(i+4), s_2(i+4), s_2(i-6), s_2(i-5), \\ &s_2(i-2), s_2(i-4), s_2(i-3), s_2(i+1), s_2(i+2), s_2(i+6), s_2(i+7), s_2(i+5), s_2(i+8), s_2(i+9)]^T\end{aligned}$$

$$(13)$$

The corresponding covariance matrix $\mathbf{C_{si'}}(i)$ (20×20) is given by

$$\begin{aligned}\mathbf{C_{si'}}(i) &= E\{\mathbf{si}'(i)\mathbf{si}'(i)^H\} \\ &= \mathbf{ai}(\varphi_i)\mathbf{ai}^H(\varphi_i) \odot \mathbf{R_{si'}}(i) + \sigma_n^2 \mathbf{I}\end{aligned}$$

$$(14)$$

$$SAR\,1 \qquad\qquad SAR\,2$$
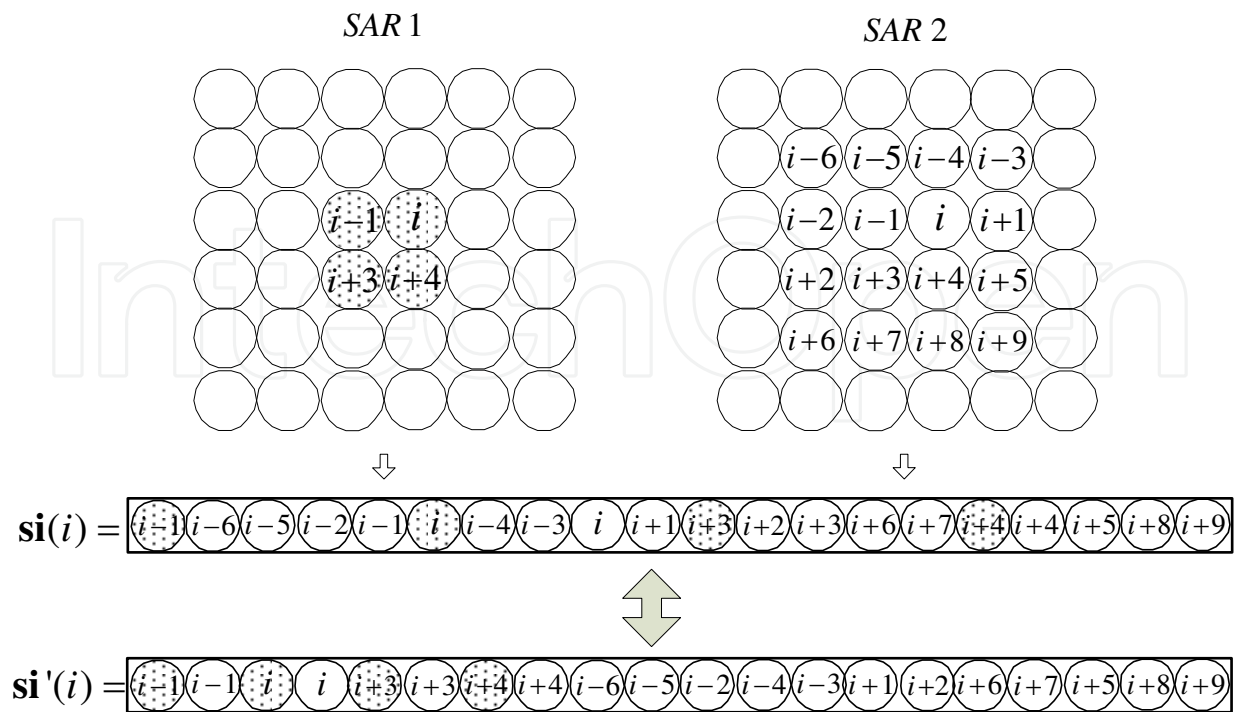

Fig. 6. Joint data vector for the accurate coregistration.

$$\mathbf{R_{si'}}(i) = \begin{bmatrix} \sigma_s^2(i-1)\mathbf{R_s}(i-1) & 0 & \cdots & 0 & \cdots & 0 \\ 0 & \sigma_s^2(i)\mathbf{R_s}(i) & & & & \vdots \\ \vdots & & \sigma_s^2(i+3)\mathbf{R_s}(i+3) & & & \\ & & & \sigma_s^2(i+4)\mathbf{R_s}(i+4) & & \\ 0 & & \sigma_s^2(i-6) & \cdots & 0 & \cdots & 0 \\ & & & \sigma_s^2(i-5) & & \\ & & & \sigma_s^2(i-2) & & \\ \vdots & & & \sigma_s^2(i-4) & & \vdots \\ & & & \sigma_s^2(i-3) & & \\ & & & \sigma_s^2(i+1) & & \\ & & & \sigma_s^2(i+2) & & \\ 0 & \cdots & 0 & \sigma_s^2(i+6) & & 0 \\ & & & \sigma_s^2(i+7) & & \\ & & & \sigma_s^2(i+5) & & \\ & & & \sigma_s^2(i+8) & & \\ 0 & \cdots & 0 & \cdots & 0 & \sigma_s^2(i+9) \end{bmatrix} \qquad (15)$$

From (14) we can see that the number of the principal eigenvalues of $\mathbf{C_{si'}}(i)$ is 16 Ref.[21]. The noise subspace dimension of the covariance matrix $\mathbf{C_{si'}}(i)$ (20×20) is 4, thus, the noise

subspace dimension of the covariance matrix $\mathbf{C_{si}}(i)$ estimated from the joint data vector $\mathbf{si}(i)$ is 4 Ref.[21].

b. Coregistration error of one pixel.

When the azimuth coregistration error is one pixel and its direction is upwards (i.e., the pixel of the image from the second satellite is shifted upwards compared to the pixel in the first satellite image), the joint data vector, $\mathbf{si}(i)$, is shown in Fig.7.

We can rearrange the elements (pixels) of $\mathbf{si}(i)$ to obtain $\mathbf{si}'(i)$ as shown in Fig.7, which does not change the eigenvalues of the corresponding covariance matrix[21]. The joint data vector $\mathbf{si}'(i)$, shown in Fig.7, can be written as

$$\mathbf{si}'(i) = [s_1(i-1), s_2(i-1), s_1(i), s_2(i), s_1(i+3), s_2(i+3), s_1(i+4), s_2(i+4), s_2(i-2), s_2(i+2),$$
$$s_2(i+1), s_2(i+5), s_2(i+6), s_2(i+7), s_2(i+10), s_2(i+11), s_2(i+8), s_2(i+9), s_2(i+12), s_2(i+13)]^T \qquad (16)$$
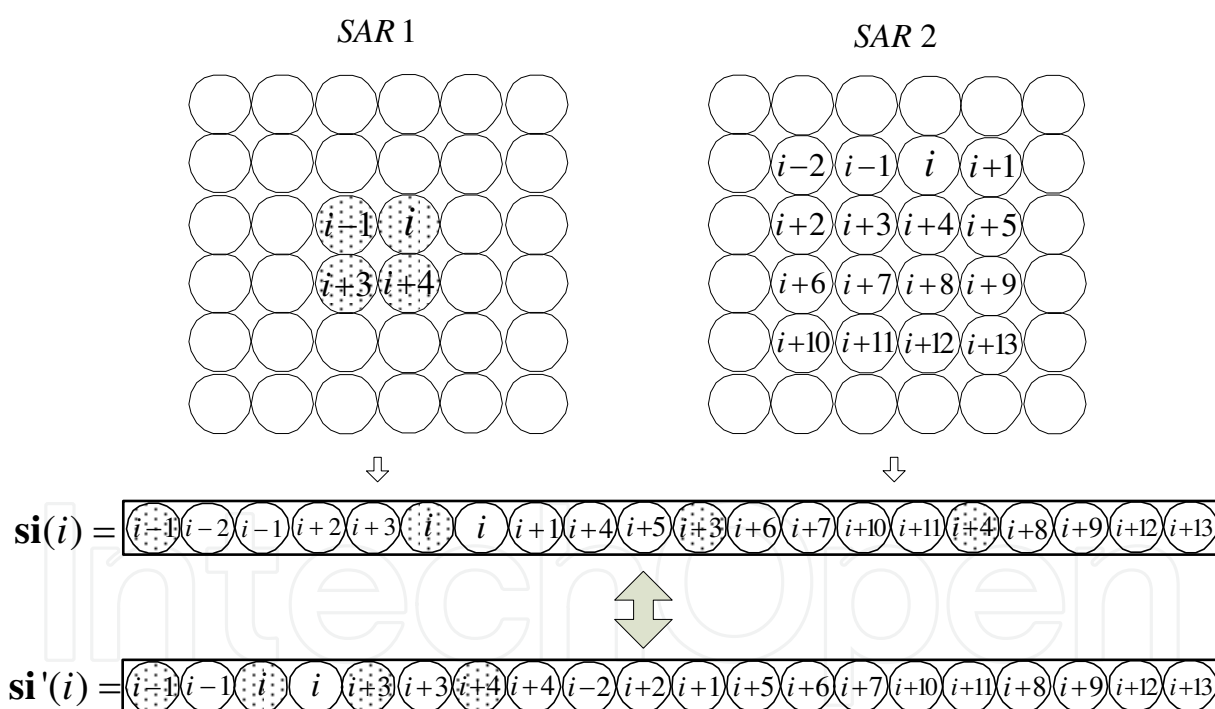

Fig. 7. Joint data vector for the coregistration error of one pixel.

The corresponding covariance matrix $\mathbf{C_{si'}}(i)$ is given by

$$\begin{aligned}\mathbf{C_{si'}}(i) &= E\{\mathbf{si}'(i)\mathbf{si}'(i)^H\} \\ &= \mathbf{ai}(\varphi_i)\mathbf{ai}^H(\varphi_i) \odot \mathbf{R_{si'}}(i) + \sigma_n^2\mathbf{I}\end{aligned} \qquad (17)$$

$$\mathbf{R_{si'}}(i) = \begin{bmatrix} \sigma_s^2(i-1)\mathbf{R_s}(i-1) & 0 & \cdots & 0 & \cdots & 0 \\ 0 & \sigma_s^2(i)\mathbf{R_s}(i) & & & & \vdots \\ \vdots & \sigma_s^2(i+3)\mathbf{R_s}(i+3) & & & & \\ & \sigma_s^2(i+4)\mathbf{R_s}(i+4) & & & & \\ 0 & \sigma_s^2(i-2) & \cdots & 0 & \cdots & 0 \\ & \sigma_s^2(i+2) & & & & \\ & \sigma_s^2(i+1) & & & & \\ \vdots & \sigma_s^2(i+5) & & & & \vdots \\ & \sigma_s^2(i+6) & & & & \\ & \sigma_s^2(i+7) & & & & \\ & \sigma_s^2(i+10) & & & & \\ 0 & \cdots & 0 & \sigma_s^2(i+11) & & 0 \\ & \sigma_s^2(i+8) & & & & \\ & \sigma_s^2(i+9) & & & & \\ & \sigma_s^2(i+12) & & & & \\ 0 & \cdots & 0 & \cdots & 0 & \sigma_s^2(i+13) \end{bmatrix} \quad (18)$$

From the above discussion, we know the noise subspace dimension of the covariance matrix $\mathbf{C_{si}}(i)$ estimated from the joint data vector $\mathbf{si}(i)$ is 4.

c. Coregistration error of μ $(0 < \mu < 1)$ pixel.

When the azimuth coregistration error is μ $(0 < \mu < 1)$ pixel and its direction is upwards (i.e., the pixel of the image from the second satellite is shifted upwards compared to the pixel in the first satellite image), the joint data vector, $\mathbf{si}(i)$,is shown in Fig.8(a).

From the literature[21], we can know that the eigenspectrum (i.e., the distribution of eigenvalues) of a covariance matrix is invariant no matter how the elements of the corresponding data vector are permuted. So we can rearrange the elements of $\mathbf{si}(i)$ to obtain $\mathbf{js}(i)$ as shown in Fig.8(b) [21], which does not change the eigenvalues of the corresponding covariance matrix. The joint data vector $\mathbf{js}(i)$, shown in Fig.8(b), can be written as

$$\mathbf{js}(i) = [s_1(i-1),s_2(i-1),s_1(i),s_2(i),s_1(i+3),s_2(i+3),s_1(i+4),s_2(i+4),s_2(i-2),s_2(i+2),$$
$$s_2(i+1),s_2(i+5),s_2(i+6),s_2(i+7),s_2(A),s_2(B),s_2(i+8),s_2(i+9),s_2(C),s_2(D)]^T \quad (19)$$

The corresponding covariance matrix $\mathbf{C_{js}}(i)$ is given by

$$\mathbf{C_{js}}(i) = E\{\mathbf{js}(i)\mathbf{js}^H(i)\}$$
$$= \mathbf{ai}(\varphi_i)\mathbf{ai}^H(\varphi_i) \odot \mathbf{R_{js}}(i) + \sigma_n^2\mathbf{I} \quad (20)$$
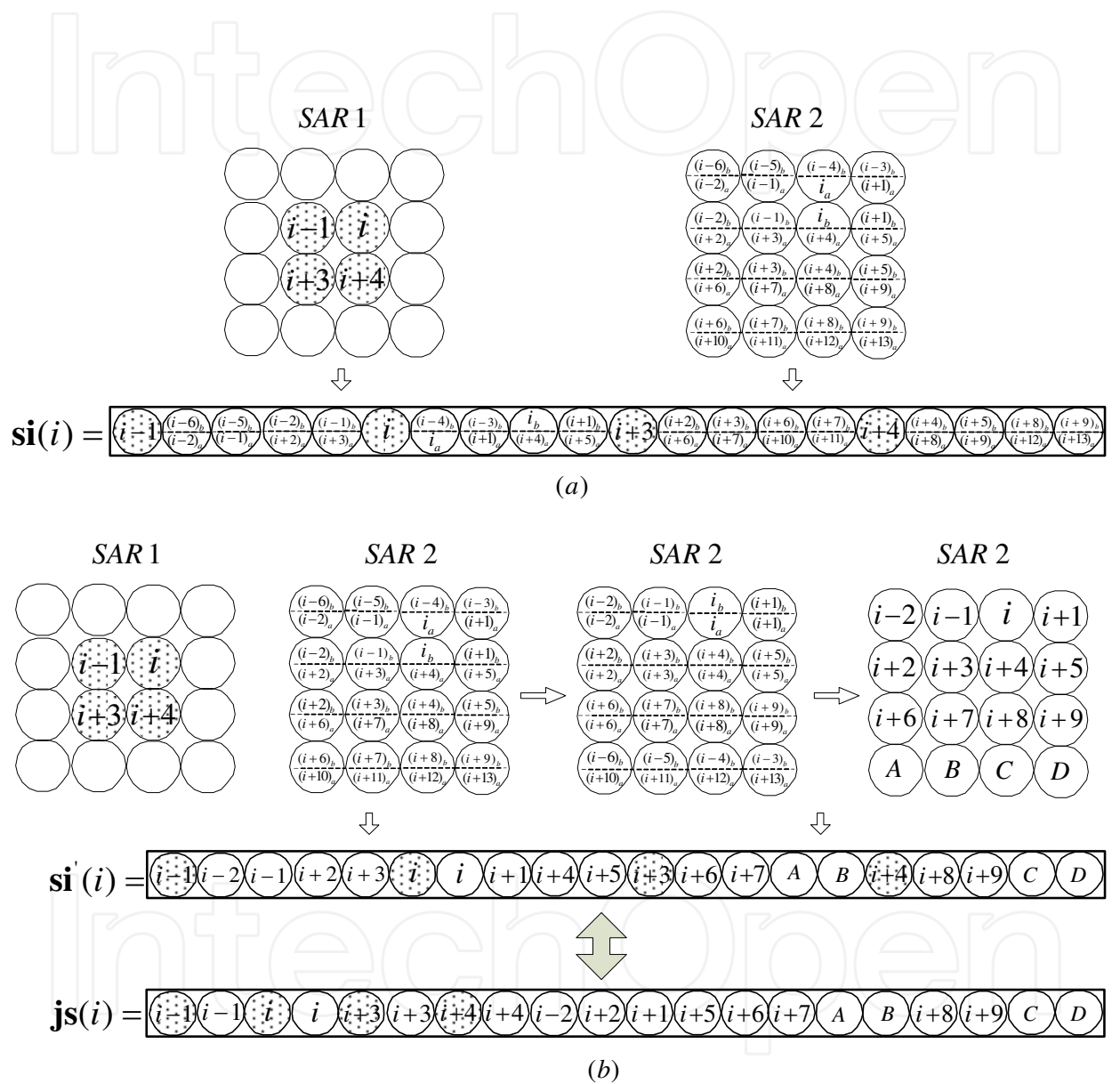
Fig. 8. Joint data vector for the coregistration error of μ pixels.

$$\mathbf{R_{js}}(i) = \begin{bmatrix} \sigma_s^2(i-1)\mathbf{R_s}(i-1) & 0 & \cdots & 0 & \cdots & 0 \\ 0 & \sigma_s^2(i)\mathbf{R_s}(i) & & & & \vdots \\ \vdots & & \sigma_s^2(i+3)\mathbf{R_s}(i+3) & & & \\ & & & \sigma_s^2(i+4)\mathbf{R_s}(i+4) & & \\ 0 & & & \sigma_s^2(i-2) & \cdots & 0 & \cdots & 0 \\ & & & \sigma_s^2(i+2) & & \\ & & & \sigma_s^2(i+1) & & \\ \vdots & & & \sigma_s^2(i+5) & & \vdots \\ & & & \sigma_s^2(i+6) & & \\ & & & \sigma_s^2(i+7) & & \\ & & & \sigma_s^2(A) & & \\ 0 & \cdots & 0 & \sigma_s^2(B) & & 0 \\ & & & \sigma_s^2(i+8) & & \\ & & & \sigma_s^2(i+9) & & \\ & & & \sigma_s^2(C) & & \\ 0 & \cdots & 0 & \cdots & 0 & \sigma_s^2(D) \end{bmatrix} \tag{21}$$

We know the noise subspace dimension of the covariance matrix $\mathbf{C_{js}}(i)$ (20×20) is 4, thus, the noise subspace dimension of the covariance matrix $\mathbf{C_{si}}(i)$ estimated from the joint data vector $\mathbf{si}(i)$ is also 4[21].

From the results derived above, we can see that: the new formulation of joint data vector proposed in this chapter has the advantage that the noise subspace dimension of the corresponding covariance matrix is independent of the coregistration error. That is to say, the noise subspace dimension of the corresponding covariance matrix with the coregistration error μ ($0 < \mu \leq 1$) pixel is the same as that of the accurate covariance matrix. Therefore, it is not required to calculate the noise subspace dimension, thus avoiding the trouble of calculating the noise subspace dimension before estimating the InSAR interferometric phase.

4.2 Summary of the modified method

In this section, we give the detailed steps for the modified interferometric phase estimation method based on subspace projection.

Step 1. Coregister SAR images. The SAR images are coarsely coregistered using the crosscorrelation information of the SAR image intensity or other strategies[1][2] after SAR imaging of the echoes acquired by each satellite. However, the allowable coregistration error of the proposed method can be very large (such as one pixel), which is useful in practice. The low coregistration accuracy requirement can greatly mitigate the complexity in image coregistration processing.

Step 2. Estimate the covariance matrix. The covariance matrix $\mathbf{C_{si}}(i)$ can be estimated by using joint data vector $\mathbf{si}(i)$ shown in Fig.5. Under the assumption that the neighboring pixels have the identical terrain height and the complex reflectivity is independent from pixel to pixel[20][21], the covariance matrix $\mathbf{C_{si}}(i)$ can be estimated by its sample covariance matrix $\hat{\mathbf{C}}_{\mathbf{si}}(i)$, i.e.,

$$\hat{\mathbf{C}}_{\mathbf{si}}(i) = \frac{1}{2K+1} \sum_{k=-L}^{L} \mathbf{si}(i+k)\mathbf{si}^H(i+k) \tag{22}$$

where $2L+1$ is the number of i.i.d. samples from the neighboring pixel pairs.

Remark 1: It is easy to obtain enough i.i.d. samples for locally flat terrains. However, an imaging terrain in practice can not be relied upon to be so flat that the adjacent pixels have the identical terrain height. If the local terrain slope is available in advance or can be estimated[20], the steering vector (i.e., the interferometric phase) variation due to the different terrain height from pixel to pixel can be compensated, which greatly enlarges the size of the sample window.

Step 3. Subspace estimation by Eigendecomposing. The estimated covariance matrix $\hat{\mathbf{C}}_{\mathbf{si}}(i)$ of the dimensions 20×20 can be eigendecomposed into

$$\hat{\mathbf{C}}_{\mathbf{si}}(i) = \sum_{m=1}^{K} \hat{\lambda}_{csi}^{(m)} \hat{\boldsymbol{\beta}}_{csi}^{(m)} \hat{\boldsymbol{\beta}}_{csi}^{(m)H} + \sum_{l=1}^{20-K} \hat{\lambda}_{csi}^{(l+K)} \hat{\boldsymbol{\beta}}_{nsi}^{(l)} \hat{\boldsymbol{\beta}}_{nsi}^{(l)H} \tag{23}$$

where K is the number of the principal eigenvalues of $\hat{\mathbf{C}}_{\mathbf{si}}(i)$, $\hat{\lambda}_{csi}^{(1)} > \hat{\lambda}_{csi}^{(2)} > \cdots > \hat{\lambda}_{csi}^{(K)} \gg \hat{\lambda}_{csi}^{(K+1)} > \cdots > \hat{\lambda}_{csi}^{(20)}$, eigenvectors $\hat{\boldsymbol{\beta}}_{nsi}^{(l)}$ ($l=1,2,\cdots,20-K$) corresponding to the smaller eigenvalues $\hat{\lambda}_{csi}^{(l+K)}$ ($l=1,2,\cdots,20-K$) span the noise subspace, i.e,

$$\mathbf{N_c} = span\left\{ \hat{\boldsymbol{\beta}}_{nsi}^{(1)}, \hat{\boldsymbol{\beta}}_{nsi}^{(2)}, \cdots, \hat{\boldsymbol{\beta}}_{nsi}^{(20-K)} \right\} \tag{24}$$

whereas the larger eigenvectors $\hat{\boldsymbol{\beta}}_{csi}^{(m)}$ ($m=1,2,\cdots,K$) corresponding to the principal eigenvalues $\hat{\lambda}_{csi}^{(m)}$ ($m=1,2,\cdots,K$) span the signal subspace, i.e.,

$$\mathbf{S_c} = span\left\{ \hat{\boldsymbol{\beta}}_{csi}^{(1)}, \hat{\boldsymbol{\beta}}_{csi}^{(2)}, \cdots, \hat{\boldsymbol{\beta}}_{csi}^{(K)} \right\} \tag{25}$$

The noise power is often estimated by

$$\hat{\sigma}_n^2 = \frac{1}{20-K} \sum_{l=1}^{20-K} \hat{\lambda}_{csi}^{(l+K)} \tag{26}$$

The joint correlation function matrix $\hat{\mathbf{R}}_{\mathbf{si}}(i)$ can be approximated as the amplitude (i.e., the absolute value) of the estimated covariance matrix $\hat{\mathbf{C}}_{\mathbf{si}}(i)$ [20], i.e.,

$$\hat{\mathbf{R}}_{\mathbf{si}}(i) = \left| \hat{\mathbf{C}}_{\mathbf{si}}(i) - \hat{\sigma}_n^2 \mathbf{I} \right| \tag{27}$$

By eigen-decomposing $\hat{\mathbf{R}}_{\mathbf{si}}(i)$, we obtain K principal eigenvectors $\hat{\boldsymbol{\beta}}_{rsi}^{(m)}$ ($m = 1, 2, \cdots, K$). As shown by (8), the same signal subspace spanned by the principal eigenvectors $\hat{\boldsymbol{\beta}}_{csi}^{(m)}$ ($m = 1, 2, \cdots, K$) of $\hat{\mathbf{C}}_{\mathbf{si}}(i)$ can be spanned by the Hadamard product vectors $\mathbf{ai}(\varphi_i) \odot \hat{\boldsymbol{\beta}}_{rsi}^{(m)}$ ($m = 1, 2, \cdots, K$), i.e.,

$$\mathbf{S_c} = span\left\{\mathbf{ai}(\varphi_i) \odot \hat{\boldsymbol{\beta}}_{rsi}^{(1)}, \mathbf{ai}(\varphi_i) \odot \hat{\boldsymbol{\beta}}_{rsi}^{(2)}, \cdots, \mathbf{ai}(\varphi_i) \odot \hat{\boldsymbol{\beta}}_{rsi}^{(K)}\right\} \tag{28}$$

Step 4. Projection of signal subspace onto noise subspace. The projection of the signal subspace onto the corresponding noise subspace is performed as follows:

$$J_3 = \sum_{m=1}^{K} \sum_{l=1}^{20-K} (\mathbf{ai}(\phi_i) \odot \hat{\boldsymbol{\beta}}_{rsi}^{(m)})^H \hat{\boldsymbol{\beta}}_{nsi}^{(l)} \hat{\boldsymbol{\beta}}_{nsi}^{(l)H} (\mathbf{ai}(\phi_i) \odot \hat{\boldsymbol{\beta}}_{rsi}^{(m)}) \tag{29}$$

where

$$\mathbf{ai}(\phi_i) = \left[1, e^{j\phi_i}, e^{j\phi_i}, e^{j\phi_i}, e^{j\phi_i}, 1, e^{j\phi_i}, e^{j\phi_i}, e^{j\phi_i}, e^{j\phi_i}, 1, e^{j\phi_i}, e^{j\phi_i}, e^{j\phi_i}, e^{j\phi_i}, 1, e^{j\phi_i}, e^{j\phi_i}, e^{j\phi_i}, e^{j\phi_i}\right]^T \tag{30}$$

The cost function given by (29) is used to estimate the terrain interferometric phase φ_i. And the minimization of J_3 can provide the optimum estimate of the interferometric phase φ_i, i.e., $\hat{\phi}_i = \varphi_i$.

Remark 2: The computational burden will be high if the minimization of J_3 is obtained via search of ϕ_i in the principal phase interval $[-\pi, +\pi]$. To reduce the computational burden, a fast algorithm to compute the minimization of J_3 is developed in Appendix B, where the closed-form solution to the estimate of ϕ_i is directly obtained by using the fast algorithm.

Using the above four steps, the terrain interferogram can be recovered after the pixel pairs of the SAR images are processed separately.

5. Numerical and experemental results

In this section we demonstrate the robustness of the modified method via subspace projection to coregistration errors by using simulated data and real data.

The simulated data are described as follows. We assume there are two formation-flying satellites in the cartwheel formation, and we select one orbit position for simulation, with an effective cross-track baseline of 281.46 m, an orbit height of 750 kilometers and an incidence angle of 45°. We use a two-dimensional window to simulate the terrain and use the statistical model to generate the complex SAR image pairs[23]. The signal-to-noise ratio (SNR) of the SAR images is 18 dB.

Here, the number of the samples to estimate the covariance matrix is 7 (in range) $\times$ 7 (in azimuth)=49.

Fig.s 9-12 compare the simulation results for various techniques and coregistration errors. Comparing Fig. 9,10 ,11and 12, we can observe that the large coregistration error heavily affects the interferograms obtained by pivoting median filtering, pivoting mean filtering and adaptive contoured window filtering. On the contrary, the large coregistration error has

almost no effect on the interferograms obtained by the modified method. We can see that the modified method in this chapter is robust to large coregistration errors (up to one pixel).

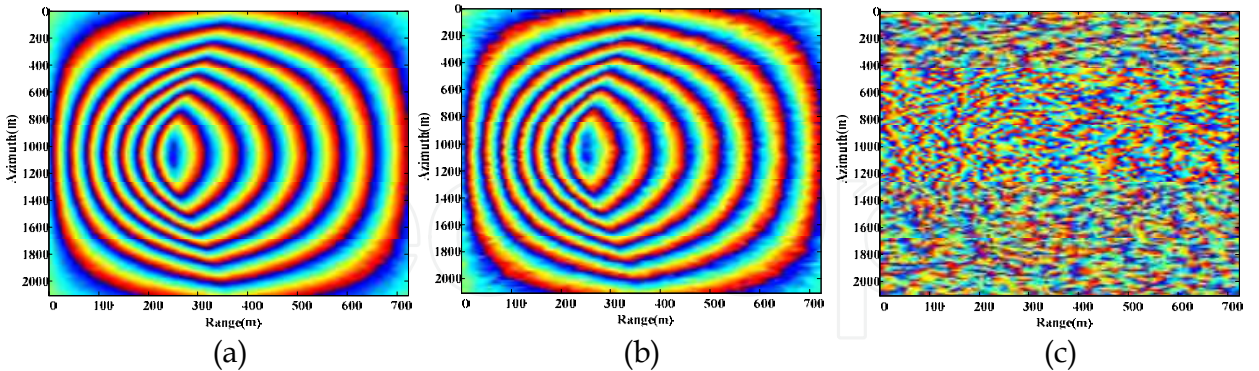(a)   (b)   (c)

Fig. 9. The interferograms obtained by the pivoting median filtering for the accurate coregistration (a), the coregistration error of 0.5 pixels (b) and the coregistration error of one pixel (c).
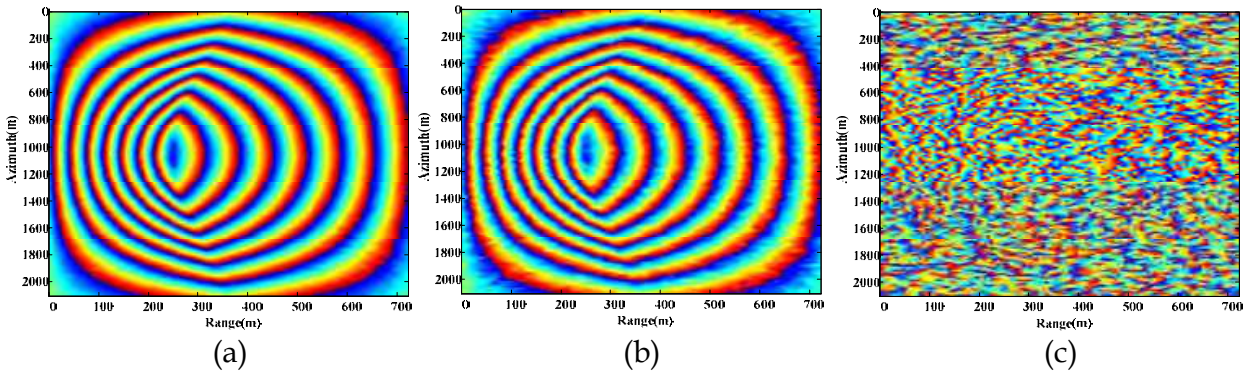

(a)   (b)   (c)

Fig. 10. The interferograms obtained by the pivoting mean filtering for the accurate coregistration (a), the coregistration error of 0.5 pixels (b) and the coregistration error of one pixel (c).

(a)   (b)   (c)
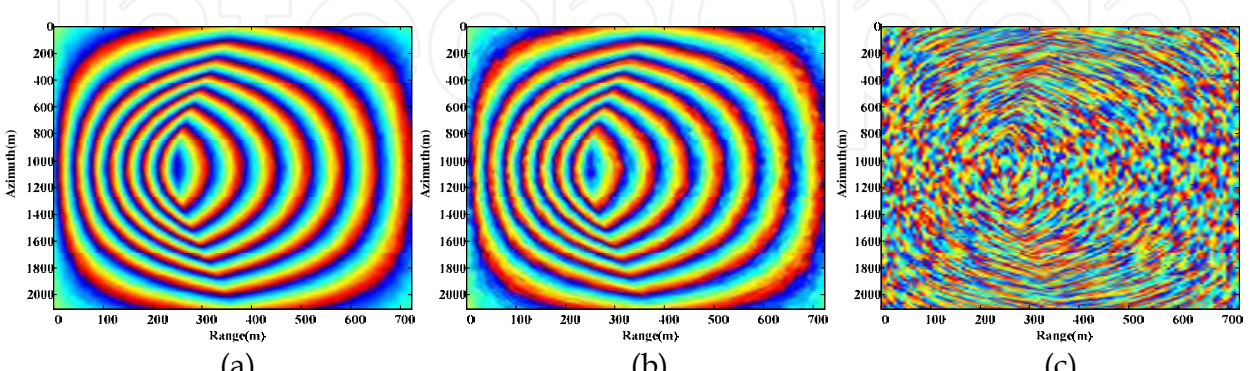
Fig. 11. The interferograms obtained by the adaptive contoured window filtering for the accurate coregistration (a), the coregistration error of 0.5 pixels (b) and the coregistration error of one pixel (c).
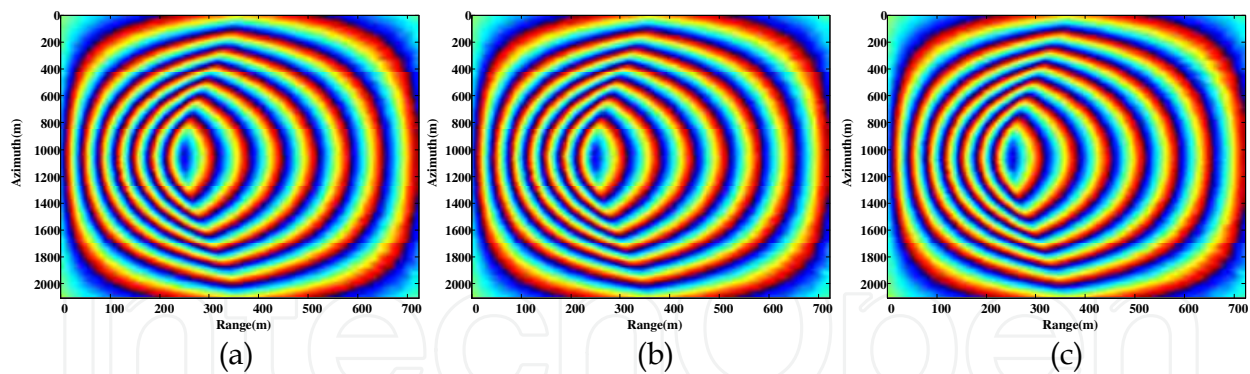
Fig. 12. The interferograms obtained by the modified method for the accurate coregistration (a), the coregistration error of 0.5 pixels (b) and the coregistration error of one pixel (c).

In the following, we will verify the validity of the modified method with the ERS1/ERS2 (European Remote Sensing 1 and 2 tandem satellites) real data.

Fig. 13 shows the interferograms generated from the ERS1/ERS2 real data. Fig.13(a) is the interferogram obtained by the conventional processing, and Fig.13(b) is that obtained by the modified method proposed in this chapter.
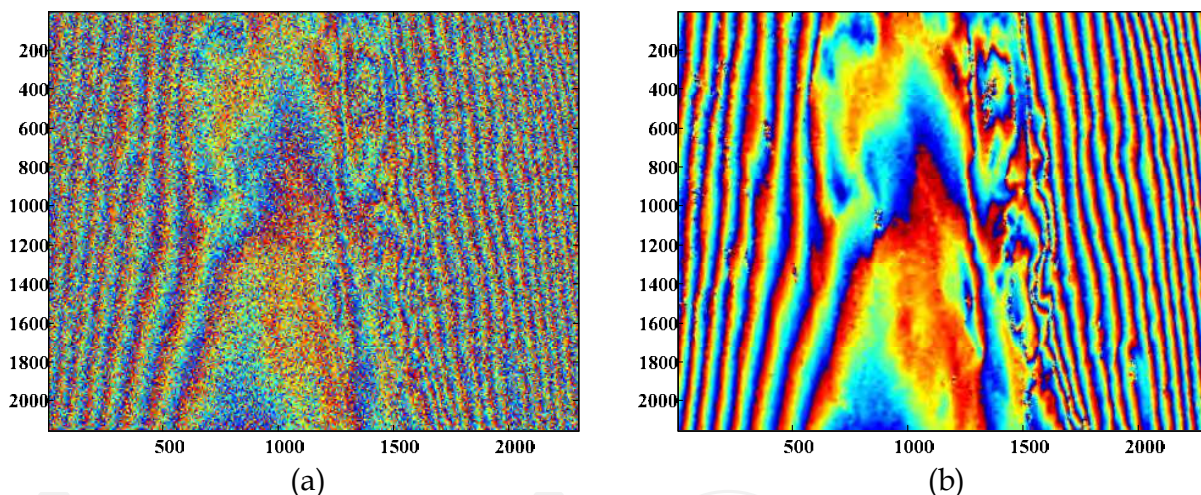

Fig. 13. The interferograms obtained by (a) the conventional processing, and (b) the modified method for the ERS1/ ERS2 real data.

6. Conclusions

In this chapter, the interferometric phase estimation method based on subspace projection and its modified method were presented. The interferometric phase estimation methods based on joint subspace projection can provide accurate estimate of the terrain interferometric phase (interferogram) even if the coregistration error reaches one pixel. Benefiting from the new formulation of joint data vector, the modified method does not need to calculate the noise subspace dimension, thus avoiding the trouble of calculating the noise subspace dimension before estimating the InSAR interferometric phase. A fast algorithm is developed to implement the modified method, which can significantly reduce the computational burden. Theoretical analysis and simulations demonstrate the efficiency of the proposed new algorithms.

7. Acknowledgement

8. Appendix A

8.1 Proof of equation (12)

For easy discussion, we assume that the structure of joint data vector $\mathbf{ss}(i)$ is shown in Fig.A.1, where circles represent SAR image pixels and i denotes the desired pixel pair whose interferometric phase is to be estimated.
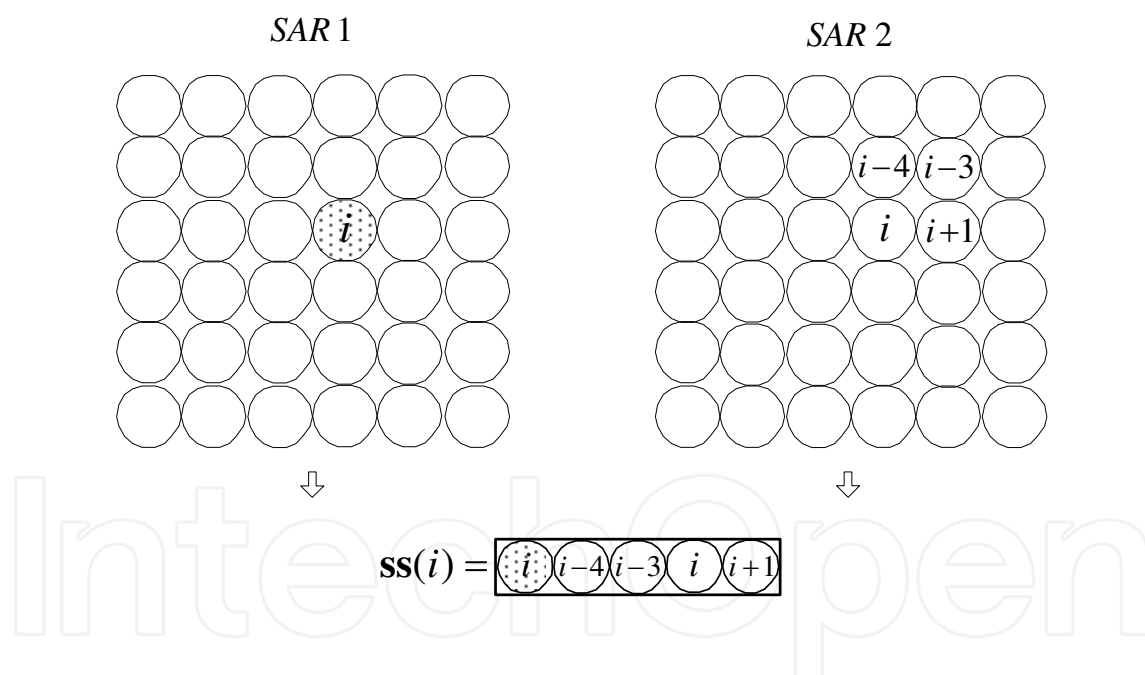

Fig. A.1. Formulation of the joint data vector $\mathbf{ss}(i)$.

The joint data vector $\mathbf{ss}(i)$, shown in Fig.A.1, can be written as

$$\mathbf{ss}(i) = [s_1(i), s_2(i-4), s_2(i-3), s_2(i), s_2(i+1)]^T \tag{A.1}$$

The corresponding covariance matrix $\mathbf{C_{ss}}(i)$ is given by

$$\mathbf{C_{ss}}(i) = E\{\mathbf{ss}(i)\mathbf{ss}^H(i)\}$$

$$= E\{[s_1(i), s_2(i-4), s_2(i-3), s_2(i), s_2(i+1)]^T [s_1(i), s_2(i-4), s_2(i-3), s_2(i), s_2(i+1)]^*\}$$

$$= \begin{bmatrix} E\{s_1(i)s_1^*(i)\}, & E\{s_1(i)s_2^*(i-4)\}, & E\{s_1(i)s_2^*(i-3)\}, & E\{s_1(i)s_2^*(i)\}, & E\{s_1(i)s_2^*(i+1)\} \\ E\{s_2(i-4)s_1^*(i)\}, & E\{s_2(i-4)s_2^*(i-4)\}, & E\{s_2(i-4)s_2^*(i-3)\}, & E\{s_2(i-4)s_2^*(i)\}, & E\{s_2(i-4)s_2^*(i+1)\} \\ E\{s_2(i-3)s_1^*(i)\}, & E\{s_2(i-3)s_2^*(i-4)\}, & E\{s_2(i-3)s_2^*(i-3)\}, & E\{s_2(i-3)s_2^*(i)\}, & E\{s_2(i-3)s_2^*(i+1)\} \\ E\{s_2(i)s_1^*(i)\}, & E\{s_2(i)s_2^*(i-4)\}, & E\{s_2(i)s_2^*(i-3)\}, & E\{s_2(i)s_2^*(i)\}, & E\{s_2(i)s_2^*(i+1)\} \\ E\{s_2(i+1)s_1^*(i)\}, & E\{s_2(i+1)s_2^*(i-4)\}, & E\{s_2(i+1)s_2^*(i-3)\}, & E\{s_2(i+1)s_2^*(i)\}, & E\{s_2(i+1)s_2^*(i+1)\} \end{bmatrix}$$

$$= \sigma_s^2(i) \begin{bmatrix} 1, & r_{12}(i,i-4)e^{-j\varphi_i}, & r_{12}(i,i-3)e^{-j\varphi_i}, & r_{12}(i,i)e^{-j\varphi_i}, & r_{12}(i,i+1)e^{-j\varphi_i} \\ r_{21}(i-4,i)e^{j\varphi_i}, & 1, & r_{22}(i-4,i-3), & r_{22}(i-4,i), & r_{22}(i-4,i+1) \\ r_{21}(i-3,i)e^{j\varphi_i}, & r_{22}(i-3,i-4), & 1, & r_{22}(i-3,i), & r_{22}(i-3,i+1) \\ r_{21}(i,i)e^{j\varphi_i}, & r_{22}(i,i-4), & r_{22}(i,i-3), & 1, & r_{22}(i,i+1) \\ r_{21}(i+1,i)e^{j\varphi_i}, & r_{22}(i+1,i-4), & r_{22}(i+1,i-3), & r_{22}(i+1,i), & 1 \end{bmatrix} + \sigma_n^2\mathbf{I}$$

$$= \begin{bmatrix} 1, & e^{-j\varphi_i}, & e^{-j\varphi_i}, & e^{-j\varphi_i}, & e^{-j\varphi_i} \\ e^{j\varphi_i}, & 1, & 1, & 1, & 1 \\ e^{j\varphi_i}, & 1, & 1, & 1, & 1 \\ e^{j\varphi_i}, & 1, & 1, & 1, & 1 \\ e^{j\varphi_i}, & 1, & 1, & 1, & 1 \end{bmatrix} \odot \left\{ \sigma_s^2(i) \begin{bmatrix} 1, & r_{12}(i,i-4), & r_{12}(i,i-3), & r_{12}(i,i), & r_{12}(i,i+1) \\ r_{21}(i-4,i), & 1, & r_{22}(i-4,i-3), & r_{22}(i-4,i), & r_{22}(i-4,i+1) \\ r_{21}(i-3,i), & r_{22}(i-3,i-4), & 1, & r_{22}(i-3,i), & r_{22}(i-3,i+1) \\ r_{21}(i,i), & r_{22}(i,i-4), & r_{22}(i,i-3), & 1, & r_{22}(i,i+1) \\ r_{21}(i+1,i), & r_{22}(i+1,i-4), & r_{22}(i+1,i-3), & r_{22}(i+1,i), & 1 \end{bmatrix} \right\} + \sigma_n^2\mathbf{I} \qquad (A.2)$$

$$= \boldsymbol{\rho}(\varphi_i)\boldsymbol{\rho}^H(\varphi_i) \odot \mathbf{R_{ss}}(i) + \sigma_n^2\mathbf{I}$$

where

$$\boldsymbol{\rho}(\varphi_i) = \left[1, e^{j\varphi_i}, e^{j\varphi_i}, e^{j\varphi_i}, e^{j\varphi_i} \right]^T \qquad (A.3)$$

$$\mathbf{R_{ss}}(i) = \sigma_s^2(i) \begin{bmatrix} 1, & r_{12}(i,i-4), & r_{12}(i,i-3), & r_{12}(i,i), & r_{12}(i,i+1) \\ r_{21}(i-4,i), & 1, & r_{22}(i-4,i-3), & r_{22}(i-4,i), & r_{22}(i-4,i+1) \\ r_{21}(i-3,i), & r_{22}(i-3,i-4), & 1, & r_{22}(i-3,i), & r_{22}(i-3,i+1) \\ r_{21}(i,i), & r_{22}(i,i-4), & r_{22}(i,i-3), & 1, & r_{22}(i,i+1) \\ r_{21}(i+1,i), & r_{22}(i+1,i-4), & r_{22}(i+1,i-3), & r_{22}(i+1,i), & 1 \end{bmatrix} \qquad (A.4)$$

So the covariance matrix $\mathbf{C_{si}}(i)$ of the joint data vector $\mathbf{si}(i)$, shown in Fig.5, can be given by

$$\mathbf{C_{si}}(i) = E\{\mathbf{si}(i)\mathbf{si}^H(i)\}$$
$$= \mathbf{ai}(\varphi_i)\mathbf{ai}^H(\varphi_i) \odot \mathbf{R_{si}}(i) + \sigma_n^2\mathbf{I} \qquad (A.5)$$

9. Appendix B

9.1 Fast algorithm for optimal interferometric phase estimation

If U, V and W are arbitrary complex column vectors, then[20]

$$(U \odot V)^H W \cdot W^H (U \odot V) = U^H \left[(W \cdot W^H) \odot (V^* \cdot (V^*)^H) \right] U \tag{B.1}$$

Using the equation (B.1), we can rewrite the cost function of (29) as

$$
\begin{aligned}
J_3 &= \sum_{m=1}^{K} \sum_{l=1}^{20-K} (\mathbf{ai}(\phi_i) \odot \hat{\boldsymbol{\beta}}_{rsi}^{(m)})^H \hat{\boldsymbol{\beta}}_{nsi}^{(l)} \hat{\boldsymbol{\beta}}_{nsi}^{(l)H} (\mathbf{ai}(\phi_i) \odot \hat{\boldsymbol{\beta}}_{rsi}^{(m)}) \\
&= \sum_{m=1}^{K} \sum_{l=1}^{20-K} \left\{ \mathbf{ai}^H(\phi_i) [(\hat{\boldsymbol{\beta}}_{nsi}^{(l)} \hat{\boldsymbol{\beta}}_{nsi}^{(l)H}) \odot (\hat{\boldsymbol{\beta}}_{rsi}^{(m)*} (\hat{\boldsymbol{\beta}}_{rsi}^{(m)*})^H)] \mathbf{ai}(\phi_i) \right\} \\
&= \mathbf{ai}^H(\phi_i) \left\{ \sum_{m=1}^{K} \sum_{l=1}^{20-K} [(\hat{\boldsymbol{\beta}}_{nsi}^{(l)} \hat{\boldsymbol{\beta}}_{nsi}^{(l)H}) \odot (\hat{\boldsymbol{\beta}}_{rsi}^{(m)*} (\hat{\boldsymbol{\beta}}_{rsi}^{(m)*})^H)] \right\} \mathbf{ai}(\phi_i)
\end{aligned}
\tag{B.2}
$$

Let $\mathbf{A} = \sum_{m=1}^{K} \sum_{l=1}^{20-K} [(\hat{\boldsymbol{\beta}}_{nsi}^{(l)} \hat{\boldsymbol{\beta}}_{nsi}^{(l)H}) \odot (\hat{\boldsymbol{\beta}}_{rsi}^{(m)*} (\hat{\boldsymbol{\beta}}_{rsi}^{(m)*})^H)]$. It can be easily proved that $\mathbf{A}$ (20×20) is a Hermitian matrix. Then (B.2) can be rewritten as

$$
\begin{aligned}
J_3 &= \mathbf{ai}^H(\phi_i) \left\{ \sum_{m=1}^{K} \sum_{l=1}^{20-K} [(\hat{\boldsymbol{\beta}}_{nsi}^{(l)} \hat{\boldsymbol{\beta}}_{nsi}^{(l)H}) \odot (\hat{\boldsymbol{\beta}}_{rsi}^{(m)*} (\hat{\boldsymbol{\beta}}_{rsi}^{(m)*})^H)] \right\} \mathbf{ai}(\phi_i) \\
&= \mathbf{ai}^H(\phi_i) \mathbf{A} \mathbf{ai}(\phi_i) \\
&= \left[\boldsymbol{\beta}^H(\phi_i), \boldsymbol{\beta}^H(\phi_i), \boldsymbol{\beta}^H(\phi_i), \boldsymbol{\beta}^H(\phi_i) \right] \begin{bmatrix} \mathbf{A}_1 & \mathbf{A}_2 \\ \mathbf{A}_3 & \mathbf{A}_4 \end{bmatrix} \begin{bmatrix} \boldsymbol{\beta}(\phi_i) \\ \boldsymbol{\beta}(\phi_i) \\ \boldsymbol{\beta}(\phi_i) \\ \boldsymbol{\beta}(\phi_i) \end{bmatrix} \\
&= \sum_{n=1}^{4} \boldsymbol{\beta}^H(\phi_i) \mathbf{A}_n \boldsymbol{\beta}(\phi_i) \\
&= \boldsymbol{\beta}^H(\phi_i) \left\{ \sum_{n=1}^{4} \mathbf{A}_n \right\} \boldsymbol{\beta}(\phi_i)
\end{aligned}
\tag{B.3}
$$

where

$$\boldsymbol{\beta}(\phi_i) = \left[1, e^{j\phi_i}, e^{j\phi_i}, e^{j\phi_i}, e^{j\phi_i} \right]^T \tag{B.4}$$

Let

$$
\mathbf{B} = \sum_{n=1}^{4} \mathbf{A}_n = \begin{bmatrix}
b_{11} & b_{12} & b_{13} & b_{14} & b_{15} \\
b_{21} & b_{22} & b_{23} & b_{24} & b_{25} \\
b_{31} & b_{32} & b_{33} & b_{34} & b_{35} \\
b_{41} & b_{42} & b_{43} & b_{44} & b_{45} \\
b_{51} & b_{52} & b_{53} & b_{54} & b_{55}
\end{bmatrix}
\tag{B.5}
$$

It can be easily proved that $\mathbf{B}$ is a Hermitian matrix, i.e.,

$$b_{1n}^* = b_{n1} \ (n = 2, 3, 4, 5) \tag{B.6}$$

so we can get $(\sum\limits_{n=2}^{5} b_{1n})^* = \sum\limits_{n=2}^{5} b_{n1}$, Let $\sum\limits_{n=2}^{5} b_{1n} = \left|\sum\limits_{n=2}^{5} b_{1n}\right| e^{j\mu}$ where $\mu = angle(\sum\limits_{n=2}^{5} b_{1n})$ and $-\pi \le \mu < \pi$.

Using (B.5) and (B.6), the cost function of (B.3) can be rewritten as

$$
\begin{aligned}
J_3 &= \boldsymbol{\beta}^H(\phi_i)\left\{\sum_{n=1}^{4}\mathbf{A}_n\right\}\boldsymbol{\beta}(\phi_i) \\
&= \boldsymbol{\beta}^H(\phi_i)\mathbf{B}\boldsymbol{\beta}(\phi_i) \\
&= \left[1, e^{-j\phi_i}, e^{-j\phi_i}, e^{-j\phi_i}, e^{-j\phi_i}\right]
\begin{bmatrix}
b_{11} & b_{12} & b_{13} & b_{14} & b_{15} \\
b_{21} & b_{22} & b_{23} & b_{24} & b_{25} \\
b_{31} & b_{32} & b_{33} & b_{34} & b_{35} \\
b_{41} & b_{42} & b_{43} & b_{44} & b_{45} \\
b_{51} & b_{52} & b_{53} & b_{54} & b_{55}
\end{bmatrix}
\begin{bmatrix}
1 \\ e^{j\phi_i} \\ e^{j\phi_i} \\ e^{j\phi_i} \\ e^{j\phi_i}
\end{bmatrix} \\
&= b_{11} + \sum_{m=2}^{5}\sum_{n=2}^{5} b_{mn} + (\sum_{n=2}^{5} b_{n1})e^{-j\phi_i} + (\sum_{n=2}^{5} b_{1n})e^{j\phi_i} \\
&= b_{11} + \sum_{m=2}^{5}\sum_{n=2}^{5} b_{mn} + ((\sum_{n=2}^{5} b_{1n})e^{j\phi_i})^* + (\sum_{n=2}^{5} b_{1n})e^{j\phi_i} \\
&= b_{11} + \sum_{m=2}^{5}\sum_{n=2}^{5} b_{mn} + (\left|\sum_{n=2}^{5} b_{1n}\right| e^{j\mu} \cdot e^{j\phi_i})^* + \left|\sum_{n=2}^{5} b_{1n}\right| e^{j\mu} \cdot e^{j\phi_i} \\
&= b_{11} + \sum_{m=2}^{5}\sum_{n=2}^{5} b_{mn} + 2\left|\sum_{n=2}^{5} b_{1n}\right|\cos(\mu + \phi_i)
\end{aligned}
\tag{B.7}
$$

Obviously, the minimization of J_3 can be obtained for $\mu + \phi_i = -\pi + 2k\pi$ (k is an integer). Since $-\pi \le \mu < \pi$ and $-\pi < \phi_i < \pi$, thus

$$
\phi_i = \begin{cases} -\pi - \mu & (\mu \le 0) \\ \pi - \mu & (\mu > 0) \end{cases}
\tag{B.8}
$$

So the closed-form solution to the estimate of ϕ_i is directly obtained by using the fast algorithm, which can significantly reduce the computational burden.

10. References

[1] P. A. Rosen, S. Hensley, I. R. Joughin, F. K. Li, S. N. Madsen, E. Rodriguez and R. M. Goldstein. Synthetic Aperture Radar Interferometry. In: Proceeding of the IEEE, 2000,88(3):333-382.

[2] R. Bamler and P. Hartl. Synthetic aperture radar interferometry. Inverse Problem, 1998,14: R1-R54.

[3] Wei Xu and Ian Cumming. A Region-Growing Algorithm for InSAR Phase Unwrapping. IEEE Trans. On GRS, 1999, 37(1): 124-134.

[4] M. Costantini. A Novel Phase Unwrapping Method based on Network Programming. IEEE Trans. On GRS, 1998, 36(3): 813-831.

[5] R. M. Goldstein, H. A. Zebker, C. L. Werner.Satellite radar interferometry : two-dimensional phase unwrapping. Radio Sci ., 1988,23(4):713 -720.

[6] M. D. Pritt and J. S. Shipman.Least-Squares Two-Dimensional Phase Unwrapping Using FFT's. IEEE Trans. On GRS ,1994, 32(3):706-708.

[7] B. Zitova and J. Flusser. Image registration methods: A survey. Image Vis. Comput., 2003,21(11): 977-1000.

[8] A. Cole-Rhodes, K. L. Johnson, J. Le Moigne, and I. Zavorin. Multiresolution registration of remote sensing imagery by optimization of mutual information using a stochastic gradient. IEEE Trans. Image Process., 2003,12:1495-1511.

[9] X. Dai and S. Khorram. A feature-based image registration algorithm using improved chain-code representation combined with invariant moments. IEEE Trans. On GRS, 1999, 37(5):2351-2362.

[10] Harold S. Stone, Michael T. Orchard, Ee-Chien Chang, and Stephen A. Martucci. A Fast Direct Fourier-Based Algorithm for Subpixel Registration of Images. IEEE Trans. On GRS, 2001, 39(10):2235-2243.

[11] Eugenio Sansosti, Paolo Berardino, Michele Manunta, Francesco Serafino, and Gianfranco Fornaro. Geometrical SAR Image Registration. IEEE Trans. On GRS, 2006, 44(10):2861-2870.

[12] Francesco Serafino. SAR Image Coregistration Based on Isolated Point Scatterers. IEEE GRS Letters, 2006, 3(3):354-358.

[13] P. H. Eichel, D. C. Ghiglia, et al. Spotlight SAR Interferometry for Terrain Elevation Mapping and Interferometric Change Detection. Sandia National Labs Tech. Report, SAND93, December 1993, pp. 2539-2546.

[14] R. Lanari, G. Fornaro, et al. Generation of Digital Elevation Models by Using SIR-C/X-SAR Multifrequency Two-Pass Interferometry: The Etna Case Study. IEEE Trans. On GRS, 1996, 34(5):1097-1114.

[15] Jong-Sen Lee, Konstantinos P. Papathanassiou, et al. A New Technique for Noise Filtering of SAR Interferometric Phase Images. IEEE Trans. On GRS, 1998, 36(5):1456-1465.

[16] Ireneusz Baran, Mike P. Stewart, Bert M. Kampes, Zbigniew Perski, and Peter Lilly. A Modification to the Goldstein Radar Interferogram Filter. IEEE Trans. On GRS, 2003, 41(9):2114-2118.

[17] Nan Wu, Da-Zheng Feng, and Junxia Li. A locally adaptive filter of interferometric phase images. IEEE GRS Letters, 2006, 3(1):73-77.

[18] Qifeng Yu, Xia Yang, Sihua Fu, Xiaolin Liu, and Xiangyi Sun. An Adaptive Contoured Window Filter for Interferometric Synthetic Aperture Radar . IEEE GRS Letters, 2007, 4(1):23-26.

[19] Hai Li, Guisheng Liao. An estimation method for InSAR interferometric phase based on MMSE criterion. IEEE Trans On GRS , 2010,48(3):1457-1469.

[20] Hai Li, Zhenfang Li, Guisheng Liao, and Zheng Bao. An estimation method for InSAR interferometric phase combined with image auto-coregistration. Science in China, Series F, 2006, 49(3): 386-396.

[21] Zhenfang Li, Zheng Bao, Hai Li, and Guisheng Liao. Image Auto-Coregistration and InSAR Interferogram Estimation Using Joint Subspace Projection. IEEE Trans. On GRS ,2006,44(2):288-297.

[22] F. Lombardini, M. Montanari, and F. Gini. Reflectivity Estimation for Multibaseline Interferometric Radar Imaging of Layover Extended Sources. IEEE Trans On SP, 2003, 51(6): 1508-1519.

[23] F. Lombardini. Absolute Phase Retrieval in a Three-element Synthetic Aperture Radar Interferometer. In: Proceeding of the 1996 CIE Int. Conf. of Radar, Beijing, China, 1996, 309-312.
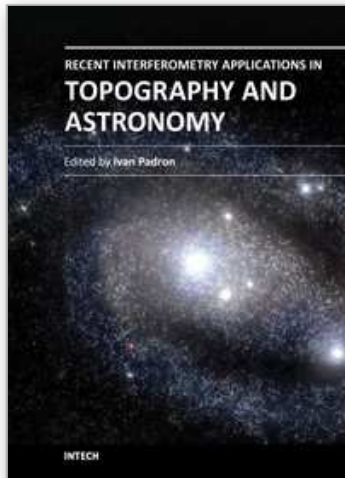
Recent Interferometry Applications in Topography and Astronomy

Edited by Dr Ivan Padron

This book provides a current overview of the theoretical and experimental aspects of some interferometry techniques applied to Topography and Astronomy. The first two chapters comprise interferometry techniques used for precise measurement of surface topography in engineering applications; while chapters three through eight are dedicated to interferometry applications related to Earth's topography. The last chapter is an application of interferometry in Astronomy, directed specifically to detection of planets outside our solar system. Each chapter offers an opportunity to expand the knowledge about interferometry techniques and encourage researchers in development of new interferometry applications.

How to reference

In order to correctly reference this scholarly work, feel free to copy and paste the following:

Hai Li and Renbiao Wu (2012). Robust Interferometric Phase Estimation in InSAR via Joint Subspace Projection, Recent Interferometry Applications in Topography and Astronomy, Dr Ivan Padron (Ed.), ISBN: 978-953-51-0404-9, InTech, Available from: http://www.intechopen.com/books/recent-interferometry-applications-in-topography-and-astronomy/robust-interferometric-phase-estimation-in-insar-via-joint-subspace-projection

INTECH

open science | open minds